Influence of Passivation on Ageing of Nano-Aluminum: Heat Flux Calorimetry and Microstructural Studies

Sreekumar Pisharath*, Zhang Fan, Ang How Ghee

AUTHOR ADDRESS: Energetics Research Institute, Nanyang Technological University, 50 Nanyang Avenue, Singapore 639798, Singapore.

AUTHOR INFORMATION

Corresponding Author

*Pisharath Sreekumar, E-mail: sreekumar@ntu.edu.sg

Highlights

- Ageing behavior of nano-aluminum is investigated by heat flux calorimetry.
- Ageing process proceeds by hydrolysis releasing 13.4kJ/g of heat.
- Organo- silane coatings act as excellent passivation barrier against ageing.
- Cumulative energy release for coated n-Al drops markedly during storage.
- Non polar organo-silane coating offers improved ageing characteristics.

ABSTRACT: Aluminum nanoparticles (n-Al) have been considered as promising fuel for incorporation in propellants and explosives to improve their performance. To prevent oxidation during storage, we investigate the effect of organic coatings on reducing oxidation of n-Al via accelerated ageing tests. The n-Al was modified with 3 different functional organic silanes. The presence of organic coatings on surface-modified n-Al was confirmed by X-ray photoelectron spectroscopy (XPS) and thermogravimetric analysis (TGA). In the accelerated ageing tests, the pristine and surface-modified n-Al were kept at elevated humidity and temperatures. The ageing process was monitored via heat flow calorimeter. The effectiveness of the organosilane coatings as barrier to hydrolysis and oxidation of n-Al was evaluated from the heat released during ageing, as well as the analysis of active Al content of the aged samples. It is found that although the pristine n-Al possesses a natural Al_2O_3 passivation layer, it cannot prevent n-Al from fully getting oxidized under the conditions tested. Organosilane coatings act as excellent barrier against diffusion of moisture preventing n-Al inside from oxidation. This study shows that all 3 kinds of organosilane-modified n-Al have much better resistance to ageing than the pristine n-Al, therefore demonstrates surface-modification of n-Al is a promising technique to extend the shelf life of n-Al during storage.

KEYWORDS: Aluminum Nanoparticles, Ageing, Heat Flow Calorimeter, Surface Modification,

1. Introduction

Nanometric Aluminium (n-Al) has been used as a fuel component in the energetic material formulations because of its high volumetric heat of combustion. As compared to micron scale counterparts, the essential characteristics of n-Al that lead to enhanced reactivity are smaller particle size and correspondingly higher surface area to volume ratio. There have been several reports on the enhancements of combustion as a result of the addition of n-Al particles to solid propellants and also to energetic nanocomposites. The reported enhancements include improvement in burn rates and shorter ignition delay [1-4].

n-Al powders undergo ageing under humid conditions by the formation of a passive layer of Aluminum hydroxide ($Al(OH)_3$) [5], reducing the overall active Al content. Lower active Al content leads to significant reduction in the volumetric heat of combustion of particles resulting in limited realization of the energy potential of the fuel. Due to the enhanced reactivity, the ageing problem is more severe in n-Al particles as compared to the micron Al particles. n-Al loses 90% of active Al content under storage at 40°C and 75% relative humidity for a period of 20days. On the other hand, micron Al loses only 25% of active Al content in the corresponding period under the same conditions [6]. The excessive oxidation of n-Al is a significant drawback associated with the usage of n-Al in energetic applications. Furthermore, the high surface area of the n-Al leads to agglomeration of the particles in the binder resulting in processability problems.

Surface functionalization of aluminum oxide surfaces by suitable modifiers has been demonstrated as a viable method not only for preventing the loss of active Al under ageing but also to improve the dispersion of n-Al particles in the binder. Representative modifiers include

different type of silanols [7], hydroxamic acids [8], carboxylic acids [9] and hydroxyl terminated polybutadiene (HTPB) polymer [10]. Surface functionalization of oxide free n-Al surfaces has also been demonstrated by self-assembly of a monolayer of pefluorinated carboxylic acid [11].

With increasing demand for n-Al in energetic materials industry, understanding the energy release during the ageing process of n-Al has become very important especially in its storage and for assessment of their fire and explosion safety. The energy release and associated kinetics during the storage of n-Al under different conditions of humidity and temperature has not been investigated.

Micro-calorimetry is an ultra-sensitive technique that enables the measurement of very small heat flow (in nano-watt range) using milligram quantities of the sample. In this paper, we investigate:

a) Energy release characteristics associated during the storage of n-Al under different conditions of humidity and temperature by microcalorimetry technique using a thermal activity monitor.

b) The effect of ageing on the microstructures of n-Al

c) Kinetics of ageing of n-Al

d) Effect of surface modifiers on the ageing properties of n-Al

2. Experimental Section

2.1 Materials

3-chloropropyltrimethoxysilane (CPTMS), sodium azide, tetrabutylammonium bromide, 3-Aminopropyl-trimethoxysilane (APTMS), 1H,1H,2H,2H perfluorodecyltriethoxysilane (PFDS), potassium fluoride (KF), sodium bromide (NaBr) and sodium chloride (NaCl) were obtained from Sigma-Aldrich. All the organic solvents were analytical grade and used as received. N-Al was provided by Armament Research, Development and Engineering Center (ARDEC) of the U.S. Army, and stored in glove box under nitrogen atmosphere. The diameter of n-Al particle is between 20-250 nm, with a mean diameter (number average) in the range 72 to 96nm as measured by scanning electron microscopy and laser diffraction respectively. The oxide layer thickness of n-Al is 3.5 nm as measured by transmission electron microscopy. The surface area calculated using the Brunauer, Emmett and Teller (B.E.T.) method was estimated to be 38.97 m^2/g. From this surface area, an average particle diameter can be estimated by assuming Al particles are nonporous and spherical with uniform size. The average particle size (APS) is calculated to be 57 nm which is in line with median diameter estimated from FESEM imaging (64 nm).

2.2 Synthesis

2.2.1 Preparation of Azidopropyltrimethoxysilane (AzPTMS)

To a 50 mL three necked round flask, CPTMS (1.5 mL, 8 mmol), sodium azide (1.1 g, 16 mmol), tetrabutylammonium bromide (0.266 g, 0.8 mmol) and toluene (10 mL) were added. The mixture was brought to 95°C and stirred for a period of 10 h. The mixture was diluted in ether, and the precipitated salts in the solution were removed by filtration. The solvent was slowly

removed via vacuum evaporator to recover azidopropyltrimethoxysilane. FTIR data (in CH_2Cl_2) : 2098 cm^{-1} ($-N_3$)

2.2.2 Surface functionalization of n-Al by silanes

Three silanes, namely 3-azidopropyltrimethoxysilane (AzPTMS), 3-aminopropyltrimethoxysilane (APTMS) and 1H,1H,2H,2H perfluorodecyltriethoxylsilane (PFDS) were used for the surface modification of n-Al. Briefly, n-Al nanoparticles (1 g) dispersed in 100 ml of toluene were stirred with 1.86 g AzPTMS, 1.793 g of APTMS and 3.05 g of PFDS respectively in a round bottom flask equipped with an overhead stirrer. The reaction was allowed to proceed at 60 °C temperature in nitrogen atmosphere, under simultaneous stirring and ultrasonication using Elma 60H ultrasonicator for 7 hrs. The unreacted silanes were washed away with toluene and acetone in several centrifugation/ultrasonication cycles, and the washed particles were dried at 50°C under vacuum. The synthesis schemes for the preparation of surface-modified n-Al particles are shown in **Scheme 1**. The modified samples were denoted as n-Al-N_3, n-Al-NH_2 and n-Al-F respectively.

2.3 Characterizations

Fourier Transform Infra-Red (FTIR) spectra of synthesized AzPTMS were recorded in a Shimadzu IR-Prestige-21 spectrometer over 4000-400 cm^{-1}using 50 scans and a resolution of 4 cm^{-1} using a sodium chloride crystal cell in transmission mode.

X-ray Photoelectron Spectroscopy (XPS) of surface-modified n-Al particles was performed using Kratos AXIS Ultra spectrometer with monochromatic Al Kα X-ray source (1486.69 eV photons) with pass energy of 80 eV for wide scan and 40 eV for element specific scan. The X-ray source was operated at a reduced power of 150 W (15 kV and 10 mA). The pressure in the

analysis chamber was maintained at 1×10^{-6} Pa or lower during each scan. The C 1s peak (285 eV) was used as a binding energy reference.

Ageing experiments were carried out under predetermined temperatures (i.e., 35°C, 42.5°C 50°C and 65°C) in isothermal mode in a thermal activity monitor (TAM III, TA instruments). TAM III is a highly sensitive micro-calorimeter capable of measuring heat flow as small as nano watt. Up to six independent calorimeters can be used simultaneously with TAM III. Temperature is controlled by a thermostat having an accuracy of 0.0001 °C. Briefly, about 10 mg each of n-Al, n-Al-NH_2, n-Al-N_3 and n-Al-F was weighed inside separate glass vials, and their exact weights were recorded. The relative humidity (RH) level of the air in the glass vials was controlled by keeping saturated salt solutions inside the vial (Figure 1). Saturated solutions of potassium fluoride (KF), sodium bromide (NaBr) and sodium chloride (NaCl) were employed to maintain RH of around 20%, 50% and 75%, respectively inside the vials [12, 13]. After the establishment of the initial baseline, the sealed glass vials were carefully inserted into the calorimeters at equilibrium position. According to the operation protocol of TAM III, the samples were allowed to equilibrate for 15 min to achieve the set temperature, before slowly lowering down to the measuring position for high sensitivity measurements. The signal was considered correct only ~ 45min after keeping the sample in the measurement position. The result is expressed in terms of heat energy release rate and cumulative heat release normalized by sample mass.

The ageing process was monitored for a maximum period of two months.

The aged samples were recovered and analyzed by X-ray diffraction (XRD), thermogravimetric analysis (TGA) and scanning electron microscopy (SEM). The powder XRD

patterns were recorded using a Bruker AXS D8 diffractometer (under ambient conditions) using a filtered Cu-Kα radiation (λ = 1.5418 Å).

TGA was performed on un-aged and aged samples using Shimadzu DTG-60H equipment. The samples were heated at a rate of 20 °C/min from room temperature to 470^0C, subsequently at the rate of 3^0C/min until 550^0C and at the rate of 20 °C/min from 550^0C until 1200^0C in a constant air flow of 50 ml/min. From the weight gain due to the reaction between aluminum and oxygen, active Al contents (by total mass) was deduced from the TGA curves according to the following equation [14]:

$$\frac{m_{Al}}{m_{O_2}} = \frac{4M_{Al}}{3M_{O_2}}\left[\frac{\Delta m}{m_0}\times 100\right] = 1.125\left[\frac{\Delta m}{m_0}\times 100\right] \quad (1)$$

where $\Delta m/m_0$ is weight gain from TGA measurement, M_{Al} and M_{O2} are the molecular weights of Al and O_2, respectively.

For both pristine and modified aluminum, the weight gain of TGA is determined from the difference between the maximum weight (after complete oxidation of Al) and minimum weight (after complete evaporation of volatile content or decomposition of organic components) divided by the initial weight of sample. For pristine Al kept under Nitrogen atmosphere, there is negligible amount of weight loss due to evaporation of volatile content or decomposition of organic components, so the initial weight is very close to the minimum weight. For this calculation, the samples are assumed to consist of only unreacted Al and Al oxide at the point of minimum weight, and there is no Al oxidation occurred prior this point of minimum weight.

Morphological studies of the samples were done using JEOL JSM-6700F Field Emission SEM operating at 10KV. The samples were coated with platinum by auto fine coater (JEOL JFC-1600).

3. Results and Discussion

3.1 Surface Characterization of Bare and Surface-modified n-Al

The XPS wide scan spectrum of bare n-Al is shown in Figure 2(a). The representative peaks corresponding to Al 2s (118 eV) and Al 2p (74 eV) [14, 15] are observed. The higher resolution Al 2P spectra of n-Al, shown in Figure 2(b), exhibits a shoulder peak at 72.5 eV along with the main peak at 74.5 eV. The shoulder peak is due to the aluminum metal and the main peak is due to the aluminum oxide. There is a substantial shift of 2eV between the aluminum and aluminum oxide peaks and the width of the aluminum oxide peak is larger than that of the aluminum peak. The peaks were curve-fitted (Figure 2(b)) to obtain the intensities of the individual aluminum and aluminum oxide peaks to calculate the thickness of the aluminum oxide layer. The oxide-film thickness, 'd' was calculated from the Al 2p peak oxide to metal ratio (I_o/I_m) using the equation [16]:

$$d(nm) = \lambda_0 \sin\theta \ln\left[\frac{C_m\lambda_m}{C_0\lambda_o} \bullet \frac{I_0}{I_m} + 1\right] \quad (2)$$

Where C_m and C_o are the volume densities of aluminum atoms in the metal and oxide respectively; λ_m and λ_o denote the inelastic mean free paths (IMFP) of the analyzed photoelectrons propagating through the metal and oxide respectively. Considering the bulk density of aluminum as 2.7 and aluminum oxide as 3.4, C_m and C_o are calculated as 0.1mol/cm^3 and 0.067mol/cm^3 and λ_m and λ_o are taken as 2.6nm and 2.8nm respectively [17]. The IMFP values are specific to Al 2p electrons emitted normal to the surface (θ=90°) of the instrument. There is good agreement between oxide layer thicknesses estimated using XPS measurement (4.2 nm) and TEM measurement (3.5 nm).

XPS wide scan spectrum of n-Al-NH_2 show signals for Si (Si 2p at 100eV and Si 2s at 150 eV) [Figure 2(c)]. For the inset, the high resolution spectrum of N 1s shows the peak at 400.5 eV indicating the presence of free amino groups from the silane layer coupled to n-Al surface. XPS

wide scan spectrum for n-Al-N_3 show similar peaks as that of n-Al-NH_2. The high resolution spectrum of N 1s [Figure 2(d)] clearly shows two peaks as a result of two different oxidation states of N atoms in the azide group. The peak at 404.5 eV is attributable to the central electron deficient nitrogen (N=<u>N</u>=N or N^+) and another peak at 400.5 eV corresponding to the two lateral nitrogens (<u>N</u>=N=<u>N</u> or N^-) [18]. The intensity of peaks due to N^+ and N^- are approximately in the ratio of 1:2. In addition, Figure 2(e) shows Cl 2p signal is absent on n-Al-N_3, indicating 3-chloropropyltrimethoxysilane has been fully converted to azidopropyltrimethoxysilane during reaction. In Figure 2(f), the XPS spectrum of n-Al-F shows a strong signal of F 1s. High resolution spectrum of F 1s confirms that the peak is at 689 eV attributed to the F-C covalent bonds on the surface of the n-Al [19, 20]. XPS investigations proved the success of our surface modification reactions using different silanes on n-Al particles to produce the respective surface-modified particles.

3.2 Quantification of surface coverage

Surface coverage in molecules/nm^2 was calculated from the estimated weight loss (X) obtained from the TGA measurements between 200°C to 400°C using the equation:

$$\text{Surface coverage (molecules/nm}^2) = \frac{X}{(1\text{-}X)\Delta M_W} \times \frac{N_{av}}{SSA} \quad (3)$$

Where X is the estimated percentage weight loss, ΔM_w is the molecular weight of the decomposed organic component in g/mol, N_{av} is the Avogadro number (6.023×10^{23}), SSA is the specific surface area of n-Al (39 m^2/g as estimated from BET surface area analysis). Typical TGA thermograms observed for all the samples are shown in Figure 3. Table 1 summarizes the weight loss observed for surface-modified n-Al samples. Among the samples, n-Al-F shows the highest weight loss because of the high molecular weight of the decomposing organic moiety.

The surface coverage of the particles by the respective surface modifiers were calculated as in the range of 1.93 to 2.44 molecules/nm^2.

3.3 Micro-calorimetry measurements on n-Al

Normalized heat flow curves for ageing of n-Al under different temperatures and relative humidity conditions are shown in Figure 4. It could be inferred from the heat flow curves that, relative humidity is having a significant effect on the ageing of n-Al. At 75%RH, exothermic peaks are observed for samples aged at all the studied temperatures of 35°C, 42.5°C, 50°C and 65°C within a 2 months period. The observed exothermic reaction is due to the hydrolysis of n-Al releasing heat of magnitude 16.95 kJ/g of Aluminum [21]. On the other hand, at 20%RH, none of the samples exhibited exothermic peaks, even for sample stored at the highest temperature of 65°C. The results indicate that humidity plays a significant role in the hydrolysis reaction of n-Al.

A representative normalized heat flow curve for n-Al aged at 50°C and 75% RH is shown in Figure 5. According to the measurement protocol of TAM III, the signal is considered correct after 45 mins of insertion of the ampoule into the calorimeter. Nie and co-workers [22] in their work on the calorimetric investigations of micron scale Aluminum-water reaction have assumed that nothing observable occurs in the earlier stages of their experiments. In our experiments, a heat flow peak was observed within the stipulated wait time of 45 mins. As observed in the inset of Figure 5, this curve is characterized by an initial phase of fast reaction followed by gradual decrease in rate to the base line. This heat flow is attributed to the instantaneous wetting of alumina layer around the n-Al particles by the humidity inside the ampoule. Huang and

Kono [23] have observed a similar peak during the heat flux calorimetric studies on the rehydration studies of alumina and ascribed it to the water adsorption on the alumina surface followed by the formation of an aquohydroxo gel.

The experiments were repeated after deactivating the 45 mins stipulation so that the heat flow signals could be analyzed for the total heat. It was measured that the hydration reaction of alumina on n-Al surface releases heat of 112J/g [43 kJ/mol normalized to 27% content of alumina shell in n-Al] at 50^0C and 75%RH. In order to compare the experimental results with theoretical heat of reaction, it is assumed that the initial stage of hydration of alumina shell produces boehmite (AlOOH) (Reaction 1).

$$Al_2O_3 + H_2O \longrightarrow 2AlOOH \qquad (1)$$

The theoretical heat of the reaction calculated by substituting the heat of formations of Al_2O_3 [-1674kJ/mole] [24] water [-285.8kJ/mole] [25] and boehmite [-996.1 kJ/mole] [26] is -32.4 kJ/mole. Boehmite is not the final product of the hydration reaction. The comparison of theoretical to experimental result concludes that complete hydration of Alumina shell has taken place. The hydration reaction progresses further leading to the formation of several intermediates before the formation of final product Bayerite [$Al(OH)_3$] [27].

As investigated by Lefevre et.al [28] the adsorption of water molecules leading to hydration of alumina proceeds through several steps. The initial phase of adsorption of water is very fast followed by an extended period of slow reaction over several hours [29]. The fast reactions occur on the surface of the alumina and the corresponding rates are related to the interfacial area. The

pore structures of alumina get blocked by the growth of hydrated oxide resulting in the hydration reactions eventually becoming limited by diffusion.

The hydration peak is followed by an induction period before the major peak of the nano-Al water reaction occurs. During the induction period, the hydration reaction of the alumina layer continues until the protective layer is significantly compromised. The hydration of the alumina shell results in local break down of the oxide layers (a process known as pitting) resulting in the formation of micro-channels [30]. For consistency, in this work, induction time is defined as the time interval between the start of the ageing experiment and the time heat flow reaches 5% of the maximum value. The variation of induction time as a function of temperature at relative humidity of 50 and 75% is shown in Figure 6. The variation of induction time is more sensitive to temperature at lower humidity condition. At 50 % RH, induction time of 29 days reduces to 1.71 day when temperature is increased from 42.5°C to 65°C. At 75% RH, induction time reduced from 3.26 days to 0.26 when temperature is increased from 35°C to 65°C. The difference in dependency of induction time with temperature at different relative humidity conditions could be attributed to the variations in the porosity of the aluminum hydroxide particles formed by the hydration of the passive alumina layer at different reaction conditions [31]. The more porous the aluminum hydroxide particles are, the shorter the induction time because higher porosity provides more micro channels through which the hydrated species will be diffusing and reacting with the n-Al core.

Induction time is an important safety consideration in the storage and handling of n-Al. It determines the safe storage period for n-Al at a given set of temperature and humidity conditions

before chemical reaction begin. It is notable that, n-Al provides a safe storage time of only 3.26 days at 35°C and 75%RH which is very common climate condition in tropical regions of the world. Therefore strict control of humidity and temperature is absolutely necessary for the safe storage of n-Al.

At the end of the induction time, the hydrated aluminum oxide has grown in thickness to the extent of reacting with the underlying Aluminum to release hydrogen gas at the aluminum boehmite interface.

$$6AlOOH + 2Al \longrightarrow 4Al_2O_3 + 3H_2 \qquad (2)$$

The pitted and porous hydrated oxide layer provides micro-channels leading to direct reaction between aluminum and moisture resulting in the major peak of the n-Al + water reaction [22].

$$2Al + 6H_2O \longrightarrow 2Al(OH)_3 + 3H_2 \qquad (3)$$

As observed in Figure 5, the reaction rate increases very fast after the induction period followed by a strong self-deceleration. The self-deceleration is related to increase in the thickness of the oxidation product layer on the surface of the n-Al and corresponding increase in the diffusion resistance of the oxide-hydroxide film towards the approach of the water molecules to the core [32]. For a given humidity, the initial rate and deceleration process becomes considerably weaker at lower temperatures and spans over a period of few days.

The total heat evolved at relative humidity of 50 and 75% is plotted in Figure 7 as a function of temperature.

The active aluminum content estimated by using equation (1) from TGA measurements is 73.8%. The cumulative heat release values for n-Al with 73.8% active aluminum are 13.35±0.53kJ/g at 50%RH and 13.38±0.29kJ/g at 75%RH averaged over the four temperatures studied. The cumulative heat release was observed to be constant with respect to change in temperature. The theoretical value reported for the complete hydration of 100% active Al to $Al(OH)_3$ is 16.95kJ/g [21]. The measured cumulative heat release is comparable to theoretical value reduced to 73.8% active aluminum i.e.16.95x0.738 = 12.5kJ/g.

The XRD patterns of the pristine n-Al and n-Al aged at 35^0C and 75%RH for a period of 26 days are shown in Figure 8.

It is observed that n-Al shows peaks at 38.4°, 44.7°, 65.1° and 78.2° which are the characteristic peaks that occur in the standard XRD pattern of bulk aluminum corresponding to the face-centered cubic (fcc) structure. The XRD pattern of pristine n-Al has significantly changed after ageing. The aged n-Al reveals double peaks at around 18.46° and 20.1° followed by significant peaks at 40.2° and 53° indicating the presence of $Al(OH)_3$ (bayerite) (indicated by the bold circles) [32]. The nonzero baseline suggests the amorphous nature of the formed $Al(OH)_3$ phases [33]. This result is consistent with the published report of formation of bayerite product during n-Al/water reaction [34].

SEM micrographs of the n-Al powders aged at 35°C and 75%RH to different extents along the normalized heat flow curve were acquired to provide information about the mechanism (Figure 9).

The designation of the micrographs corresponds to the labelled locations of the heat flow curve. Clearly, significant changes in the microstructure are observed for n-Al during the progression of ageing process. Before the beginning of the ageing experiment (Figure 9a), n-Al particles have a spherical morphology with smooth surface. After the induction period (Figure 9b), the surface of the n-Al particles becomes rough probably due to the formation of the micro channels on the surface by hydration of the alumina layer. The particles appear to be agglomerated and the spherical morphology of the particles is still retained. After crossing the peak of the ageing reaction (Figure 9c), n-Al particle become much more agglomerated and starts to change from spherical to rod shaped particles with some of the particles still retaining the spherical morphology. This change in morphology indicates the formation of the hydrated oxidation product as a result of the reaction of water with n-Al. Morphology of the n-Al particles doesn't change after crossing the peak to the end of the reaction [Figure 9(d)]. A magnified view of same micrograph (Figure 9(e)) indicates that the rod shaped particles have a shape consistent with bayerite.

3.4 Kinetics of n-Al-water reaction

Isoconversional analysis was performed to study the kinetics of the nano-Al water reaction. Briefly, the isoconversional principle states that the reaction rate is function of the temperature only at constant extent of reaction (α) [35]. Applications of isoconversional methods to thermally stimulated reactions have been extensively reviewed in literature [36]. Isoconversional methods provide a reaction model free estimate of activation energy as a function of extent of reaction. In

this work, Friedman's and Vyazovkin's advanced isoconversional methods were used to study the kinetics.

Friedman's method is based on the equation

$$\ln\left(\frac{d\alpha}{dt}\right)_{\alpha,i} = \ln[A_\alpha f(\alpha)] - \frac{E_\alpha}{RT_{\alpha i}} \quad (4)$$

Where the index '*i*' refers to individual temperature of isothermal programs and $T_{\alpha,i}$ is the temperature at which the extent of conversion (α) is reached at the i^{th} temperature. At any given value of α, activation energy (E_α) is estimated as the slope of the plot of $\ln(d\alpha/dt)_{\alpha,i}$ against $1/T_{\alpha,i}$.

Vyazovkin's advanced isoconversional method is based on the equation

$$\Phi(E_\alpha) = \sum_{i}^{n}\sum_{j\neq 1}^{n}\frac{J[E_\alpha, T_i(t_\alpha)]}{J[E_\alpha, T_j(t_\alpha)]} \quad (5)$$

where $J[E_\alpha, T(t_\alpha)]$ is defined as:

$$J[E_\alpha, T(t_\alpha)] = \int_{t_{\alpha-\Delta\alpha}}^{t_\alpha} \exp\left[\frac{-E_\alpha}{RT(t)}\right]dt \quad (6)$$

and $T_i(t)$ is the isothermal temperature program. The integral (Eq.6) was solved numerically by using 'quadv' function in MATLAB 2010. The integration is carried over small segments of extent of conversion, where the E_α is assumed constant only within a small interval of $\Delta\alpha$.

E_α was obtained by minimizing the function (Eq.5) for each value of α using 'fminunc' function for unconstrained optimization in MATLAB.

For the calorimetric measurements, the extent of reaction (α) is defined as:

$$\alpha = \frac{H_t}{H_R} \quad (7)$$

Where H_t is the heat flow of the reaction until time t and H_R is the total heat of the reaction obtained by the integration of the micro-calorimetric curve. As clear from Figure 7, the total heat of the reaction is approximately constant over the range of studied temperatures.

The extent of reaction (α) versus time profiles for the ageing reaction of n-Al at 75% RH and temperatures of 35°C, 42.5°C, 50°C and 65°C are shown in Figure 10. All the curves exhibit sigmoidal α-t dependence with a characteristic induction period. At 50°C and 65°C, the induction period is too small to be visible due to the large time scale of the plot.

The activation energy dependencies estimated by Friedman's method and Vyazovkin's advanced isoconversional method are shown in Figure 11. Both the methods yield similar profiles for the activation energy dependencies with higher values estimated for Vyazovkin's method. No drastic change in the activation energy was observed during the progress of the n-Al-water reaction. The activation energy dependency demonstrates an increase of E_α by 8 kJ/mol in the range of $[0.1<\alpha<0.25]$ followed by a plateau region $[0.3<\alpha<0.7]$ and gradual decrease $[0.7<\alpha<0.9]$. The shoot up in the activation energy profile after $\alpha>0.9$ could be due to the discrepancy in the α–t data towards the end of the reaction which is also reflected in the higher magnitude of error bars in the Friedman's analysis.

The initial increase in the activation energy could be attributed to competitive reactions of nano-Al with: a) boehmite (hydrated aluminum oxide) at the Al/hydrated alumina interface; b) with

moisture seeping through the micro-channels in the hydrated hydroxide layer to release hydrogen [intermediate oxidation reactions]. Once the hydrated aluminum oxide has sufficiently grown in size [known as hydroxide ripening], the approach of water molecules to the underlying nano Aluminum surface becomes diffusion controlled resulting in the decrease in the reaction rate. As observed from Figure 9(c), the morphology of n-Al particles changes from spherical to rod shaped particles after crossing the peak of ageing reaction. The particles start to stick together resulting in effective loss of surface area leading to decrease in the reaction rate. The decreasing dependence of the E_α on conversion after α=0.4 is the indication of the diffusion control of the reaction.

Based on the calorimetric analysis, the n-Al hydration reaction mechanism could be summarized as in Scheme 2.

The isoconversional treatment of the kinetic data reflects the multiple processes namely the intermediate oxidation and hydroxide ripening occurring during the n-Al water reaction after the hydration of the alumina shell.

3.5 Microcalorimetry measurements on surface-modified n-Al

Harshest condition (65°C, 75%RH) was employed to study the ageing characteristics of surface-modified n-Al using the heat flux calorimeter. The ageing experiments were monitored until the peak for n-Al was fully developed for a given set of conditions. Normalized heat flow curves for the ageing of different surface-modified n-Al are shown in Figure 12.

The heat flow peak was drastically reduced in surface coated n-Al particles, due to the protection offered by the coverage of organic functional groups to the approach of water molecules to alumina surface. The magnitude of heat flow is extremely low over the period of storage. This result indicates that the surface modifying agents are effective in protecting n-Al from ageing reactions even in harshest of the environments. Mechanistically, the surface modifiers provide an impermeable protective layer for the moisture to access the alumina layer on the surface of n-Al. The mechanism is substantiated by the higher magnitude of heat flow recorded for APTMS surface modifier containing the surface amino groups having higher chemical affinity towards water. Among the modifiers, n-Al modified with 3-aminopropyltrimethoxysilane (n-Al-NH_2) show higher magnitude of heat flow at the beginning of the measurement. The heat flow measured for n-Al particles modified with azidopropyltrimethoxysilane (n-Al-N_3) and perfluorodecyltriethoxylsilane (n-Al-F) are very minimal, indicating the efficient protective effect of azidopropyltrimethoxysilane and perfluorodecyltriethoxysilane coatings on n-Al towards ageing.

The cumulative heat released for n-Al during ageing at 75%RH is compared with surface modified particles in Figure 13.

It is noted that, the magnitude of cumulative heat release reaches a range of 13.1 kJ/g even at 35°C and 70%RH. This climatic condition is quite common in tropical countries. Having passivated with an amino silane, the cumulative energy release decreases significantly to 491 J/g for storage at similar conditions. The cumulative energy release decreases to 140 J/g when nano-

Al is coated with an azido silane and further to 44J/g when coated with fluoro silane. The cumulative energy release scales down with the increasing hydrophobicity of the chemical groups attached to the silane. This result indicates that surface passivation approach is successful in improving the storage safety of n-Al by significantly reducing the cumulative heat release during storage at a given temperature and humidity.

3.6 Preservation of active aluminum

TGA technique was used to estimate the active aluminum content of the surface-modified n-Al powders after ageing. As shown in Figure 13, upon heating to 350°C in air, powders show initial weight loss due to the loss of volatile organic components from the surface modifiers and water.

On further heating, oxidation of n-Al proceeds in two distinct steps separated by a plateau at 600°C to 750°C as observed by Johnson and co-workers [37]. Complete oxidation of the powders is indicated by the attainment of constant weight and also by the change in the color of the residue from grey to white. The weight gain observed on complete oxidation was used to calculate active aluminum content of the sample. The active aluminum content of n-Al before ageing experiment was estimated as 73.8 % from TGA. n-Al completely changes it chemical nature to hydrated aluminum under ageing as indicated by totally different TGA profile for aged n-Al. The weight loss for aged n-Al (from room temperature to 1200°C is 34.0%, which is consistent with the theoretical weight loss from $Al(OH)_3$ to Al_2O_3 (34.6%). On the other hand, surface-modified n-Al particles retain TGA oxidation profile of n-Al with a lower weight gain as compared to the fresh n-Al. The active aluminum content for n-Al-NH_2, n-Al-N_3 and n-Al-F are estimated to be 65.6%, 67.2% and 55.6%, respectively, from weight gain in TGA experiments.

These active aluminum contents by total mass is higher than the values reported for surface passivation of nano Al with organic capping, such as 40% for oleate-capped n-Al [38], 35% for epoxide polymer-capped n-Al [39] and 15% for perfluoroalkyl carboxylic-capped n-Al [11]. After ageing, the active aluminum content drop to 62.4%, 62.9% and 55.9%, respectively. TGA results shows no significant difference among n-Al-NH_2, n-Al-N_3 and n-Al-F in their capability to retain active aluminum, and vast majority of the active Al contents are preserved by this surface modifier under the harshest condition tested.

It is worthy to note the limitation of estimation via TGA. There is overlapping between the end of weight loss (around 400°C) and the onset of weight gain due to Al oxidation (around 300°C). Therefore, underestimation of weight gain and active aluminum content, especially for samples having higher weight loss, are inevitable.

4. Conclusions

In summary, we investigated the ageing behavior of nano-Al under controlled temperature and humidity conditions by the technique of micro-calorimetry. It was observed that, ageing of nano-Al is very sensitive to variation in humidity at a given storage temperature. The cumulative heat release during storage at 35^0C and 75%RH was estimated as 13.4 kJ/g. Mechanistic investigations indicate that the ageing process proceeds by hydrolysis reaction and the final product is Bayerite. Isoconversional analysis of kinetic data was performed by Friedman's and Vyazovkin's advanced methods. The dependence of activation energy on conversion showed the intermediate oxidation and hydroxide ripening steps involved in the nano-Al hydrolysis. In this work, we also demonstrated the effectiveness of three organo-silane modifiers namely;

aminopropyltrimethoxysilane, azidopropyltrimethoxysilane and perfluorodecyltriethoxysilane on preventing the ageing of nano-Al in terms of significant drop in the cumulative energy release during storage. It is observed that, surface modifiers with non-polar chemical groups provide better resistance against ageing at a given temperature and humidity condition. The active Aluminum (Al^0) content per total mass of nanoparticles is well preserved from ageing with an average surface coverage of 2molecules of surface modifiers per nm^2 of the nanoparticles.

REFERENCES

[1] B.S. Bockmon, M.L. Pantoya, S.F. Son, B.W. Asay, J.T. Mang, Combustion velocities and propagation mechanisms of metastable interstitial composites, J. Appl. Phys., 98 (2005) 064903.
[2] A. Dokhan, E.W. Price, J.M. Seitzman, R.K. Sigman, The effects of bimodal aluminum with ultrafine aluminum on the burning rates of solid propellants, Proceedings of the Combustion Institute, 29 (2002) 2939-2946.
[3] J.J. Granier, M.L. Pantoya, Laser ignition of nanocomposite thermites, Combust. Flame, 138 (2004) 373-383.
[4] K. Jayaraman, K.V. Anand, S.R. Chakravarthy, R. Sarathi, Effect of nano-aluminium in plateau-burning and catalyzed composite solid propellant combustion, Combust. Flame, 156 (2009) 1662-1673.
[5] L. Meda, G. Marra, L. Galfetti, F. Severini, L. De Luca, Nano-aluminum as energetic material for rocket propellants, Materials Science & Engineering C: Biomimetic and Supramolecular Systems, 27 (2007) 1393-1396.
[6] M. Cliff, F. Tepper, V. Lisetsky, Ageing characteristics of Alex(R) nanosize aluminium, 37th Joint Propulsion Conference and Exhibit, (2001).
[7] L. Houssiau, P. Bertrand, ToF-SIMS study of organosilane self-assembly on aluminum surfaces, Appl. Surf. Sci., 175 (2001) 351-356.
[8] J.P. Folkers, C.B. Gorman, P.E. Laibinis, S. Buchholz, G.M. Whitesides, R.G. Nuzzo, Self-Assembled Monolayers of Long-Chain Hydroxamic Acids on the Native Oxide of Metals, Langmuir, 11 (1995) 813-824.
[9] M.E. Karaman, D.A. Antelmi, R.M. Pashley, The production of stable hydrophobic surfaces by the adsorption of hydrocarbon and fluorocarbon carboxylic acids onto alumina substrates, Colloids and Surfaces A: Physicochemical and Engineering Aspects, 182 (2001) 285-298.
[10] L. Guo, W. Song, M. Hu, C. Xie, X. Chen, Preparation and reactivity of aluminum nanopowders coated by hydroxyl-terminated polybutadiene (HTPB), Appl. Surf. Sci., 254 (2008) 2413-2417.

[11] R.J. Jouet, A.D. Warren, D.M. Rosenberg, V.J. Bellitto, K. Park, M.R. Zachariah, Surface passivation of bare aluminum nanoparticles using perfluoroalkyl carboxylic acids, Chem. Mater., 17 (2005) 2987-2996.
[12] L. Greenspan, Humidity fixed points of binary saturated aqueous solutions, Journal of Research of the National Bureau of Standards Section A: Physics and Chemistry, 81 (1977) 89-96.
[13] L.B. Rockland, Saturated Salt Solutions for Static Control of Relative Humidity between 5° and 40°C, Anal. Chem., 32 (1960) 1375-1376.
[14] M. Fogliazza, L. Sicard, P. Decorse, A. Chevillot-Biraud, C. Mangeney, J. Pinson, Powerful Surface Chemistry Approach for the Grafting of Alkyl Multilayers on Aluminum Nanoparticles, Langmuir, 31 (2015) 6092-6098.
[15] B.W. McMahon, J. Yu, J.A. Boatz, S.L. Anderson, Rapid Aluminum Nanoparticle Production by Milling in NH3 and CH3NH2 Atmospheres: An Experimental and Theoretical Study, ACS applied materials & interfaces, 7 (2015) 16101-16116.
[16] M.R. Alexander, G.E. Thompson, X. Zhou, G. Beamson, N. Fairley, Quantification of oxide film thickness at the surface of aluminium using XPS, Surf. Interface Anal., 34 (2002) 485-489.
[17] Y.A. Atmane, L. Sicard, A. Lamouri, J. Pinson, M. Sicard, C. Masson, S. Nowak, P. Decorse, J.Y. Piquemal, A. Galtayries, C. Mangeney, Functionalization of Aluminum Nanoparticles Using a Combination of Aryl Diazonium Salt Chemistry and Iniferter Method, J. Phys. Chem. C, 117 (2013) 26000-26006.
[18] A.C. Gouget-Laemmel, J. Yang, M.A. Lodhi, A. Siriwardena, D. Aureau, R. Boukherroub, J.N. Chazalviel, F. Ozanam, S. Szunerits, Functionalization of Azide-Terminated Silicon Surfaces with Glycans Using Click Chemistry: XPS and FTIR Study, J. Phys. Chem. C, 117 (2013) 368-375.
[19] H. Touhara, F. Okino, Property control of carbon materials by fluorination, Carbon, 38 (2000) 241-267.
[20] Y.S. Lee, Syntheses and properties of fluorinated carbon materials, J. Fluorine Chem., 128 (2007) 392-403.
[21] V. Rosenband, A. Gany, Application of activated aluminum powder for generation of hydrogen from water, Int. J. Hydrogen Energy, 35 (2010) 10898-10904.
[22] H.Q. Nie, M. Schoenitz, E.L. Dreizin, Calorimetric investigation of the aluminum-water reaction, Int. J. Hydrogen Energy, 37 (2012) 11035-11045.
[23] C.C. Huang, H.O. Kono, Granulation and rehydration of rehydratable alumina powders, Industrial & Engineering Chemistry Research, 28 (1989) 910-919.
[24] C.E. Holley, E.J. Huber, The Heats of Combustion of Magnesium and Aluminum, J. Am. Chem. Soc., 73 (1951) 5577-5579.
[25] F.D. Rossini, The heat of formation of water, Proceedings of the National Academy of Sciences of the United States of America, 16 (1930) 694-699.
[26] Q. Chen, W. Zeng, Calorimetric determination of the standard enthalpies of formation of gibbsite, Al(OH)3(cr), and boehmite, AlOOH(cr), Geochim. Cosmochim. Acta, 60 (1996) 1-5.
[27] W. Mišta, J. Wrzyszcz, Rehydration of transition aluminas obtained by flash calcination of gibbsite, Thermochim. Acta, 331 (1999) 67-72.
[28] G. Lefevre, M. Duc, P. Lepeut, R. Caplain, M. Fedoroff, Hydration of gamma-alumina in water and its effects on surface reactivity, Langmuir, 18 (2002) 7530-7537.

[29] W.P. Ma, P.W. Brown, Mechanisms of reaction of hydratable aluminas, J. Am. Ceram. Soc., 82 (1999) 453-456.
[30] B.C. Bunker, G.C. Nelson, K.R. Zavadil, J.C. Barbour, F.D. Wall, J.P. Sullivan, C.F. Windisch, M.H. Engelhardt, D.R. Baer, Hydration of passive oxide films on aluminum, J. Phys. Chem. B, 106 (2002) 4705-4713.
[31] N.S. Shaytura, M.N. Laritchev, O.O. Laritcheva, E.I. Shkolnikov, Study of texture of hydroxides formed by aluminum oxidation with liquid water at various activation techniques, Current Applied Physics, 10 (2010) S66-S68.
[32] V.G. Ivanov, M.N. Safronov, O.V. Gavrilyuk, Macrokinetics of oxidation of ultradisperse aluminum by water in the liquid phase, Combustion Explosion and Shock Waves, 37 (2001) 173-177.
[33] L. Soler, A.M. Candela, J. Macanás, M. Muñoz, J. Casado, Hydrogen generation by aluminum corrosion in seawater promoted by suspensions of aluminum hydroxide, Int. J. Hydrogen Energy, 34 (2009) 8511-8518.
[34] C.E. Bunker, M.J. Smith, K.A.S. Fernando, B.A. Harruff, W.K. Lewis, J.R. Gord, E.A. Guliants, D.K. Phelps, Spontaneous Hydrogen Generation from Organic-Capped Al Nanoparticles and Water, ACS applied materials & interfaces, 2 (2010) 11-14.
[35] S. Vyazovkin, Chapter 13 Isoconversional kinetics, in: E.B. Michael, K.G. Patrick (Eds.) Handbook of Thermal Analysis and Calorimetry, Elsevier Science B.V., 2008, pp. 503-538.
[36] S. Vyazovkin, Isoconversional Methodology, in: Isoconversional Kinetics of Thermally Stimulated Processes, Springer International Publishing, 2015.
[37] C.E. Johnson, S. Fallis, A.P. Chafin, T.J. Groshens, K.T. Higa, I.M.K. Ismail, T.W. Hawkins, Characterization of nanometer- to micron-sized aluminum powders: Size distribution from thermogravimetric analysis, J. Propul. Power, 23 (2007) 669-682.
[38] K.A.S. Fernando, M.J. Smith, B.A. Harruff, W.K. Lewis, E.A. Guliants, C.E. Bunker, Sonochemically Assisted Thermal Decomposition of Alane N,N-Dimethylethylamine with Titanium (IV) Isopropoxide in the Presence of Oleic Acid to Yield Air-Stable and Size-Selective Aluminum Core-Shelll Nanoparticles, J. Phys. Chem. C, 113 (2009) 500-503.
[39] D.W. Hammerstroem, M.A. Burgers, S.W. Chung, E.A. Guliants, C.E. Bunker, K.M. Wentz, S.E. Hayes, S.W. Buckner, P.A. Jelliss, Aluminum Nanoparticles Capped by Polymerization of Alkyl-Substituted Epoxides: Ratio-Dependent Stability and Particle Size, Inorg. Chem., 50 (2011) 5054-5059.

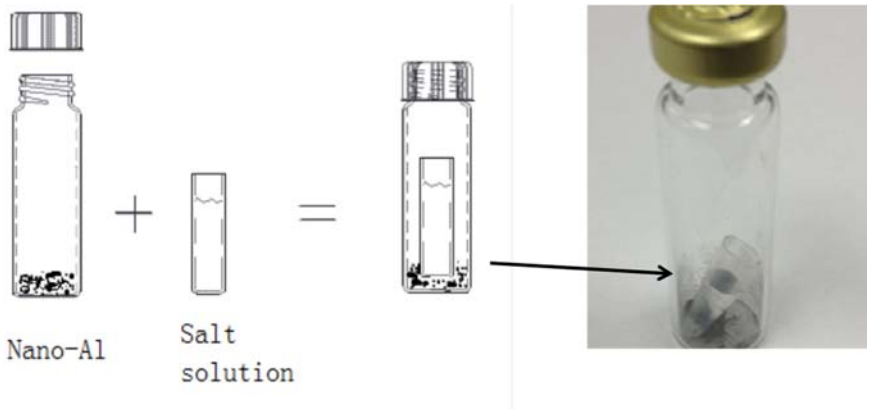

Figure 1. Experimental set up for the ageing studies done in TAMIII

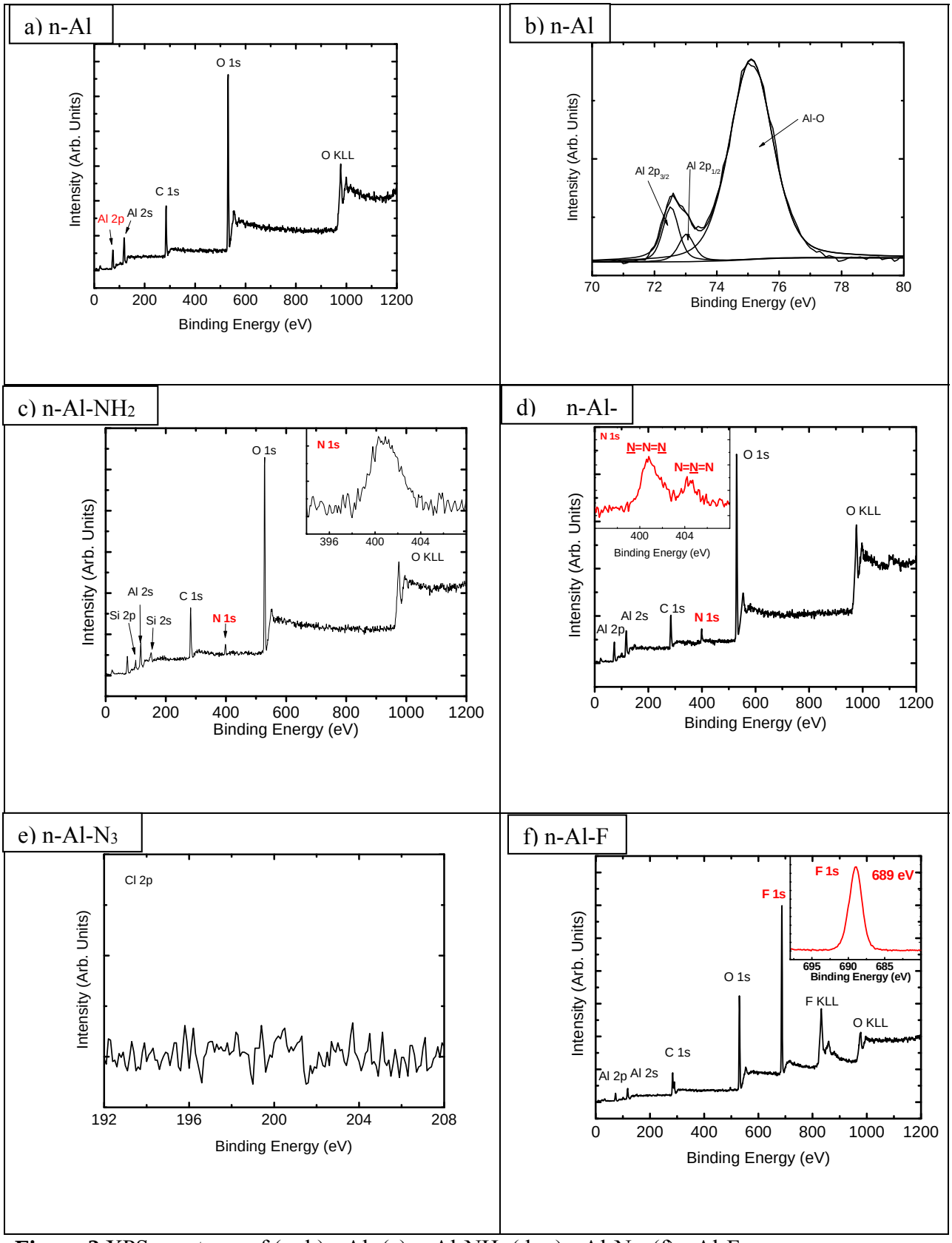

Figure 2 XPS spectrum of (a- b)n-Al; (c) n-Al-NH; (d- e)n-Al-N_3; (f)n-Al-F.

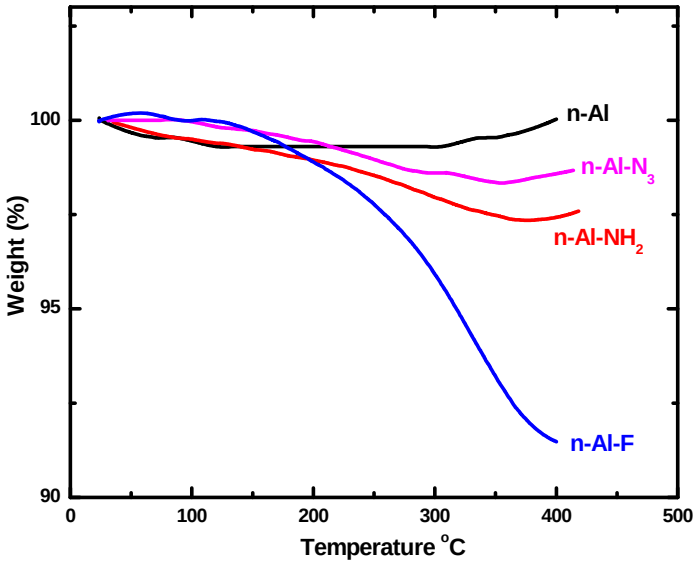

Figure 3. TGA of n-Al and surface modified nanoparticles; n-Al-NH_2, n-Al-N_3 and n-Al-F.

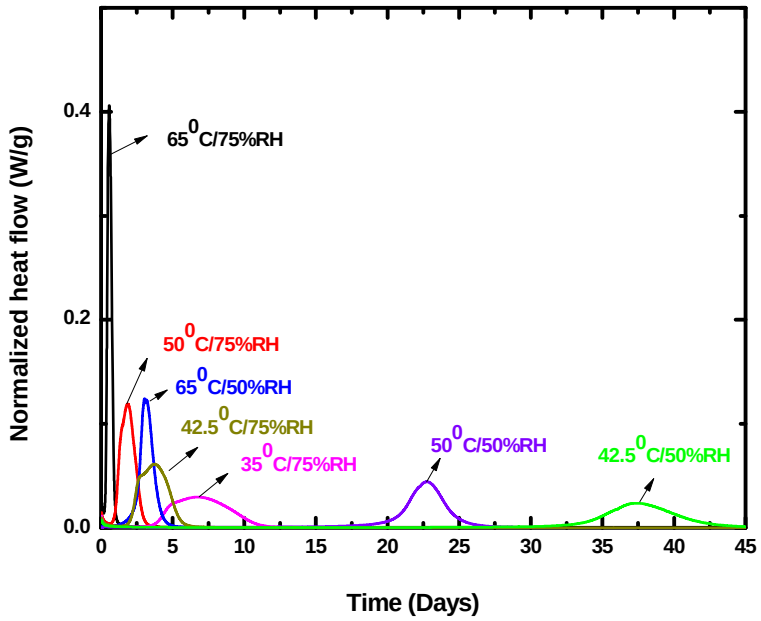

Figure 4. Normalized heat flow curves for n-Al at different temperature and relative humidity.

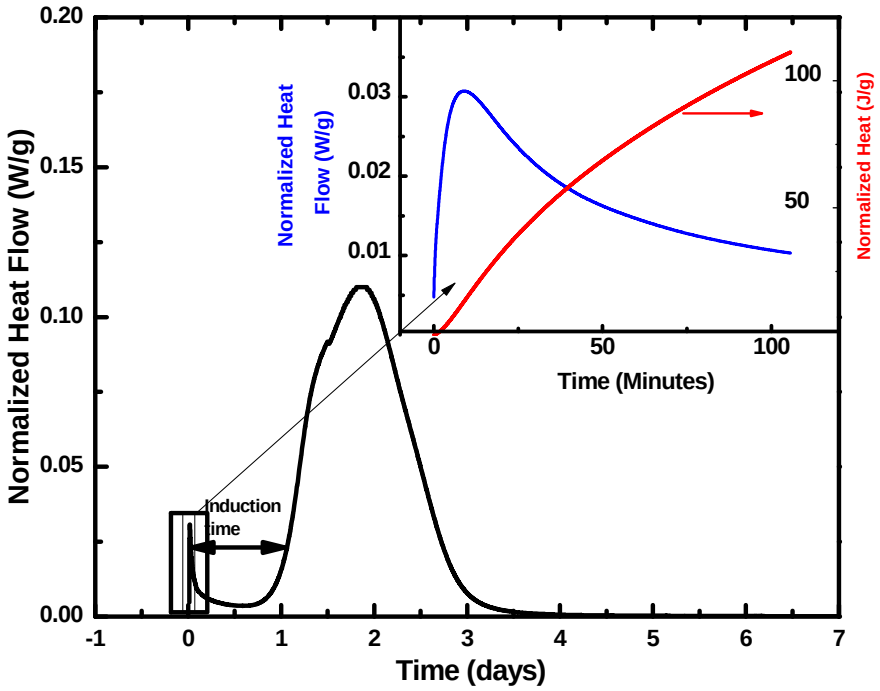

Figure 5. Normalized heat flow curve for the ageing of n-Al at 50°C and 75%RH. Inset graph shows the enlarged region of the heat flow and normalized heat during hydration reaction of the alumina shell of n-Al.

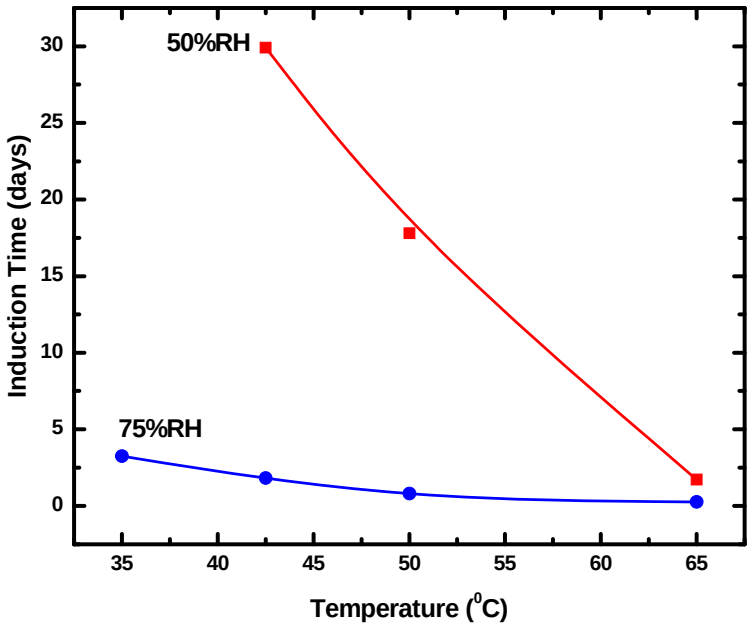

Figure 6. Effect of temperature on induction time at different humidity conditions for the ageing of nano-Al.

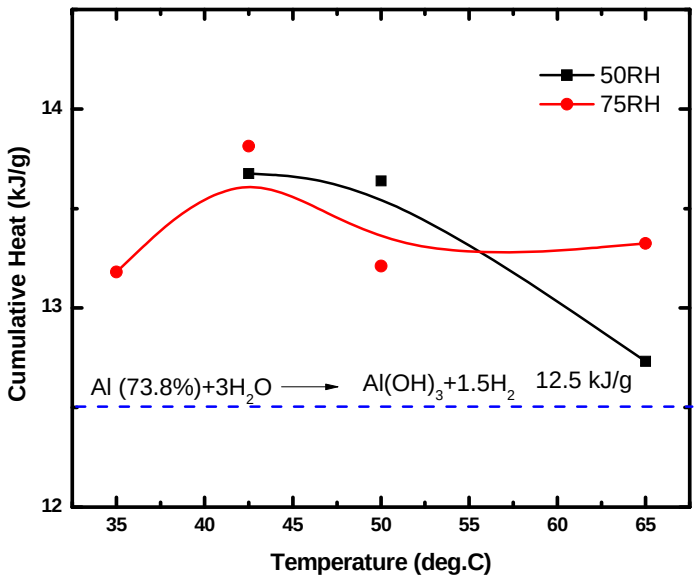

Figure 7. Effect of temperature on cumulative heat release at different humidity conditions for the ageing of nano-Al. The theoretical value for the hydration of Aluminum with 73.8% active Al is also shown. Solid lines serve as a guide to the eye.

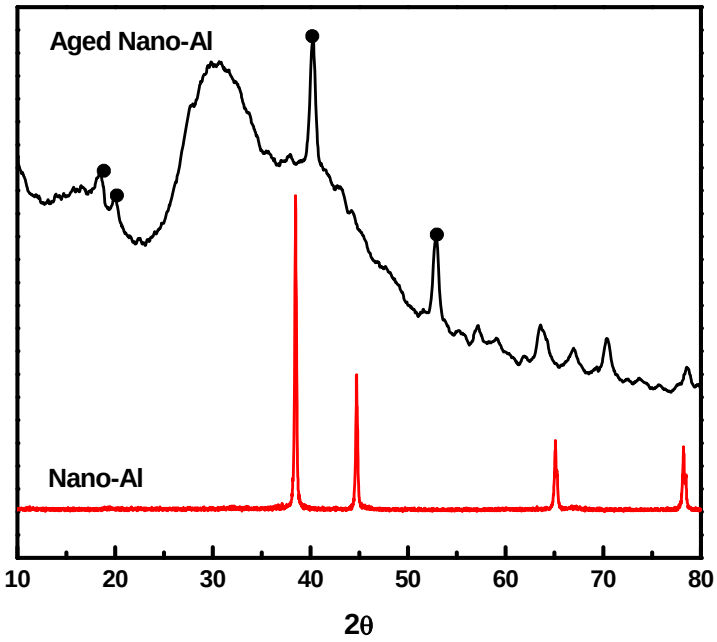

Figure 8. XRD patterns of the pristine n-Al and aged n-Al. The bold circles on aged nano-Al XRD pattern indicate the characteristic peaks of Bayerite.

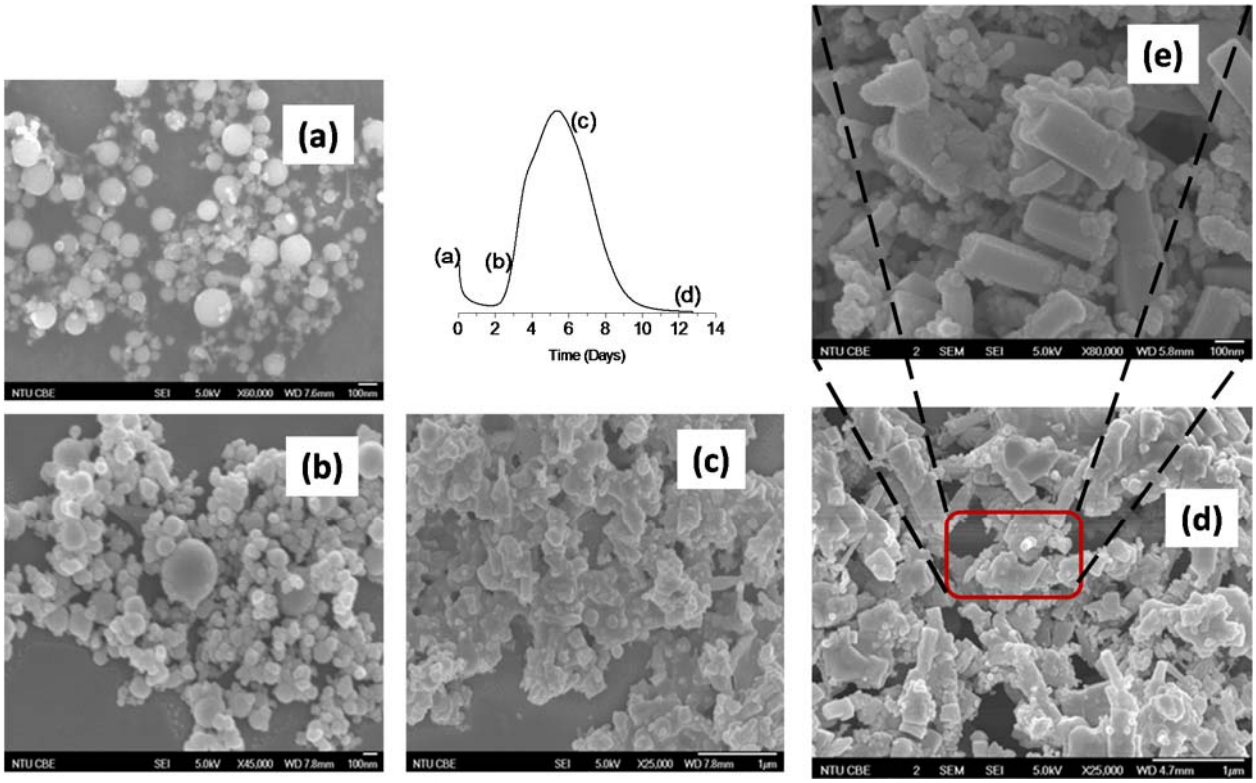

Figure 9. SEM micrographs of n-Al powders during different extent of ageing at 35°C and 75%RH. Figure 9(e) is the magnified version of figure 9(d) indicating that the rod shaped particles have an ordered monoclinic shape.

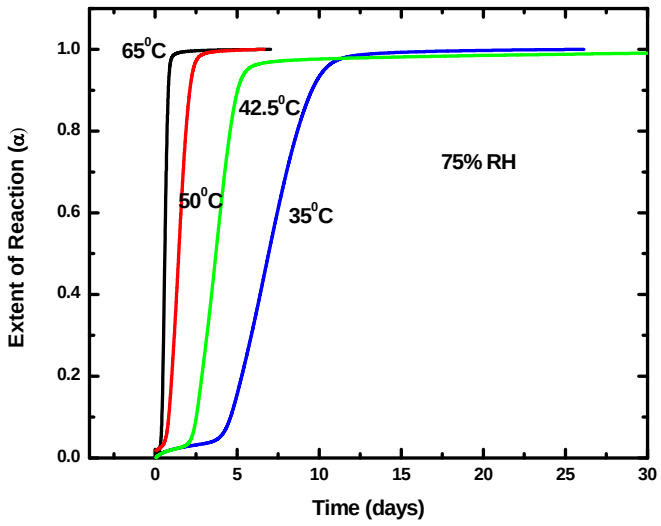

Figure 10. Extent of reaction versus time profiles for ageing of n-Al at 75%RH.

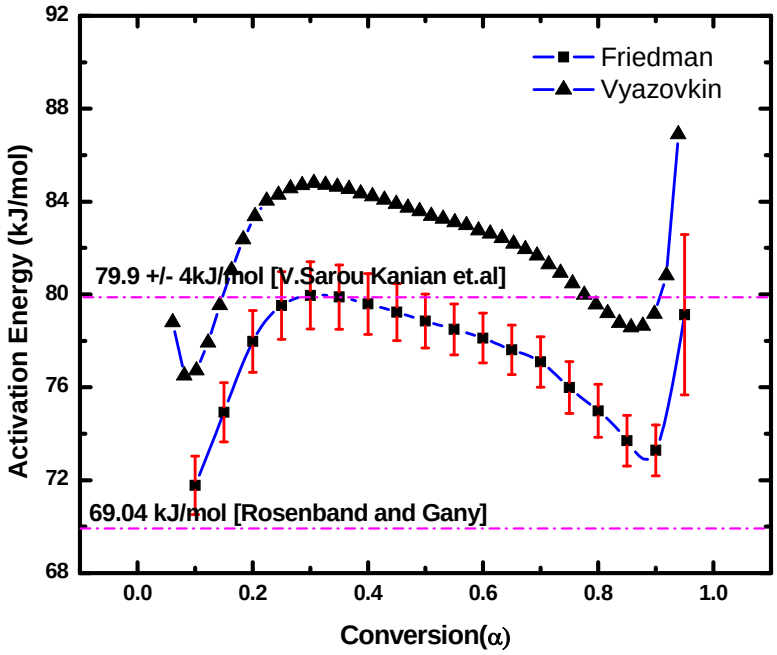

Figure 11. Activation energy dependency for the n-Al-water reaction estimated by Friedman's method and Vyazovkin's advanced isoconversional method. Literature reported activation energy values from model fitting method are also shown for comparison.

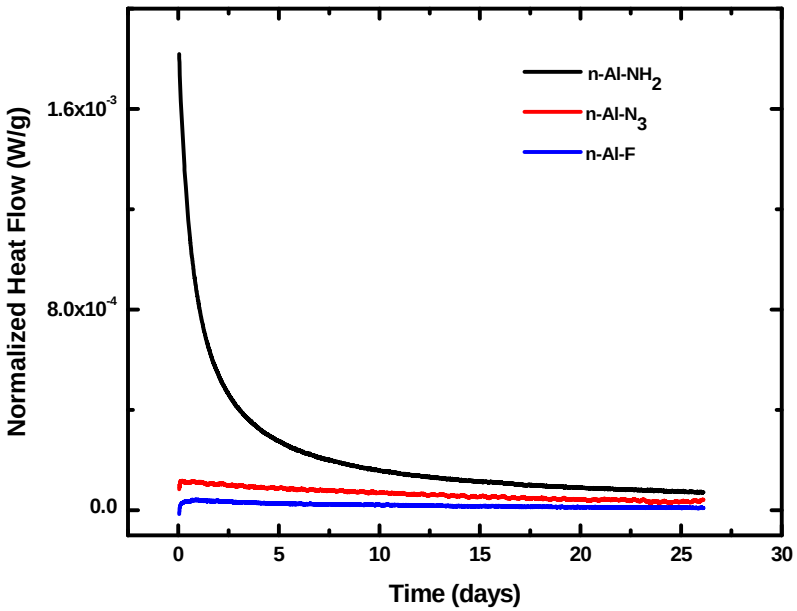

Figure 12. Normalized heat flow curves for n-Al-NH_2, n-Al-N_3 and n-Al-F at 65°C and 75%RH

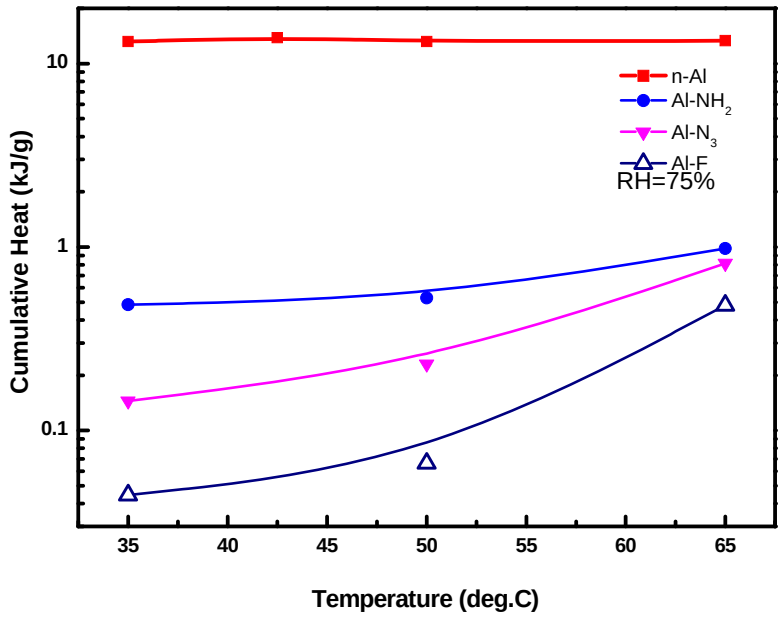

Figure 13: Cumulative heat released during ageing for n-Al and surface modified n-Al particles as a function of temperature at 75%RH. The solid lines serve as a guide to the eye.

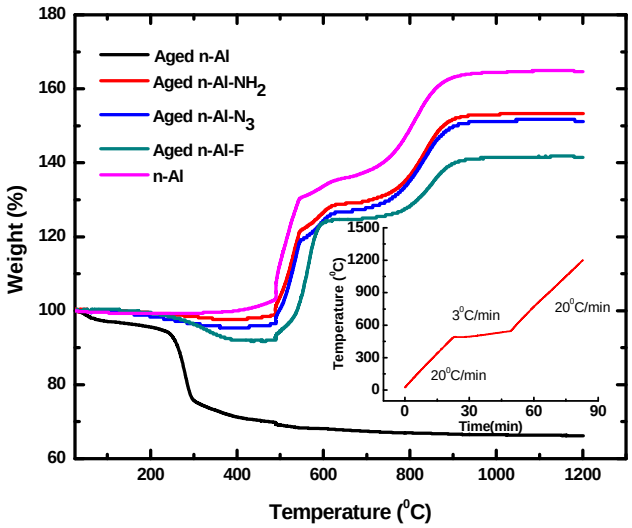

Figure 14. TGA curves of n-Al and surface-modified n-Al after ageing at 65°C and 75%RH.The time temperature profiles used for TGA measurements is shown as inset.

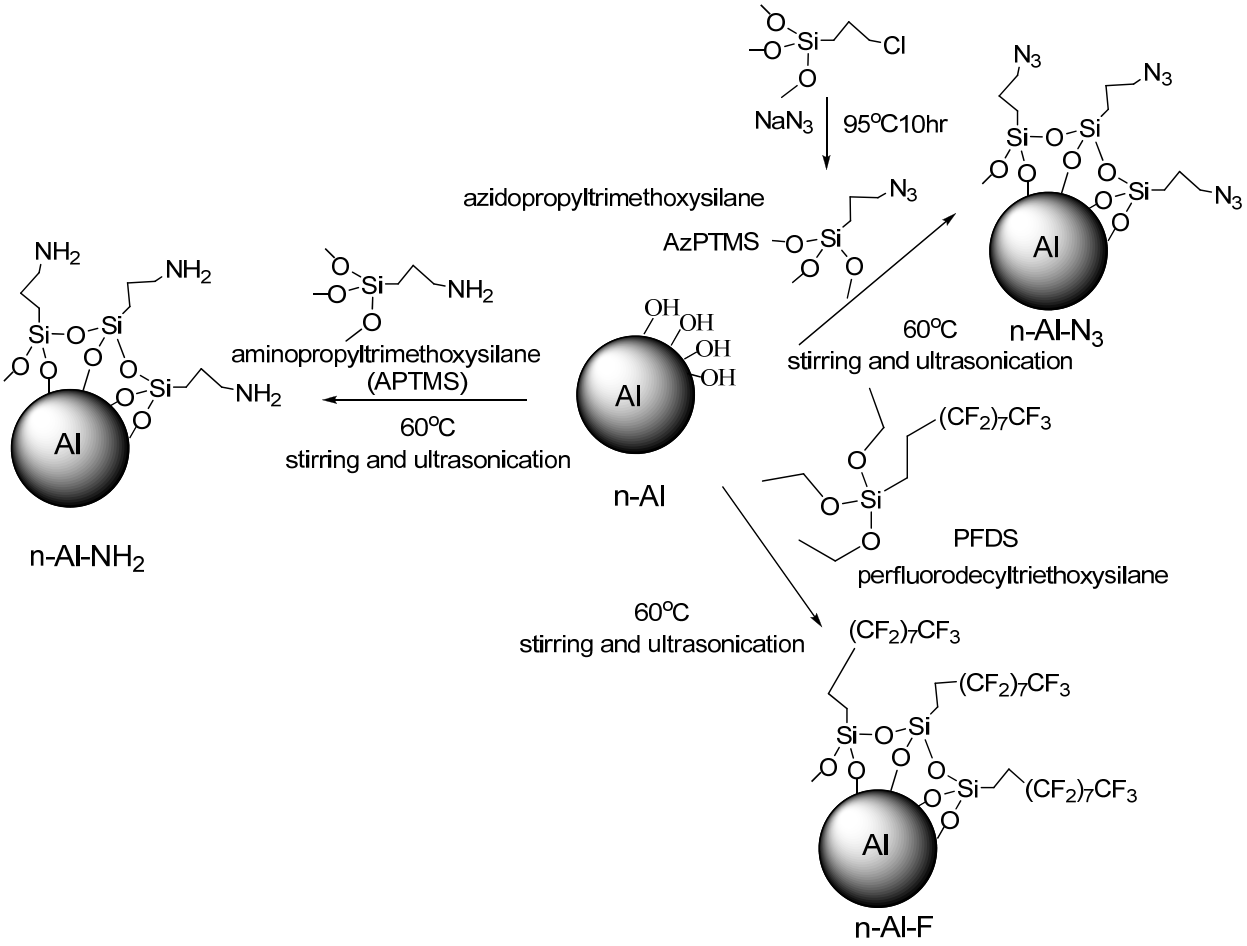

Scheme 1. Reaction scheme for surface modification of n-Al using different silanes

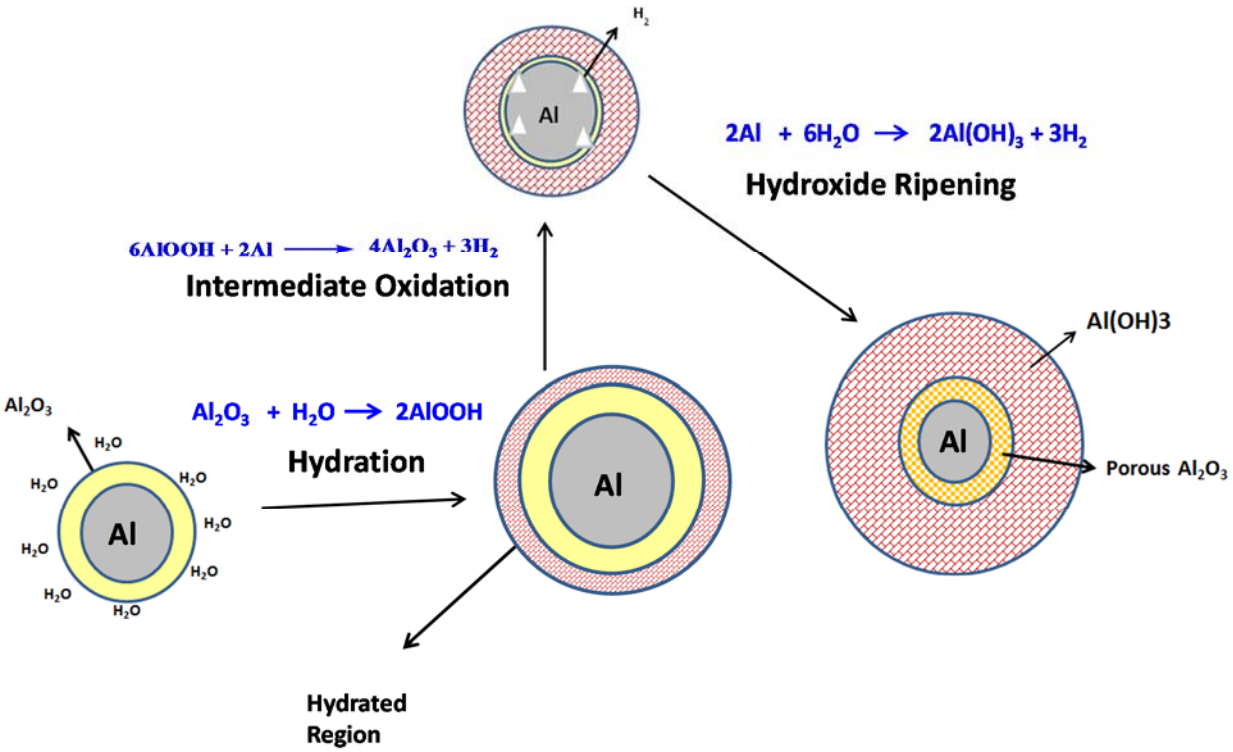

Scheme 2 Reactions involved in the nano-Al hydration process

Table 1. Weight loss observed for surface-modified n-Al samples

Sample	Weight loss (%)	Δ MW (g/mol)	Surface coverage (molecules/nm^2)
n-Al-NH_2	2.192	58	1.93
n-Al-N_3	1.556	84	1.19
n-Al-F	8.785	447	2.44